

AT 2025abao: the fourth luminous red nova in M 31

A. Reguitti^{1,2,*}, A. Pastorello¹, G. Valerin¹, F. D. Romanov³, A. Siviero^{4,1}, Y.-Z. Cai^{5,6}, S. Ciroi⁴, N. Elias-Rosa^{1,7}, T. Iijima¹, E. Kankare⁸, N. Koivisto⁸, T. Kravtsov⁸, E. Mason⁹, K. Matilainen⁸, A. C. Mura^{4,1}, P. Ochner^{4,1}, T. M. Reynolds^{8,10}, M. D. Stritzinger¹¹

(Affiliations can be found after the references)

Accepted . Received 15 February 2026; in original form 7 November 2025

ABSTRACT

We present photometric and spectroscopic observations of the luminous red nova (LRN) AT 2025abao, the fourth discovered in M 31. The LRN, associated with the AGB star WNTR23bzdiq, was discovered during the fast rise following the minimum phase. It reached the peak at $g = 15.1$ mag ($M_g = -9.5 \pm 0.1$ mag), and then it settled onto a long-duration plateau in the red bands, lasting 70 days, while it was slowly linearly declining in the blue bands. The object showed similarities at peak with the canonical LRNe V838 Monocerotis, V1309 Scorpii, and with the faint and fast-evolving AT 2019zhd, the third LRN in M31, though the later evolution is different. Spectroscopically, AT 2025abao evolved as a canonical LRN: the early spectra present a blue continuum with narrow Balmer lines in emission; at peak, the spectral continuum has cooled to a yellow colour, with a photospheric temperature of 6000 K. Balmer lines have weakened while absorption lines from metals (Fe I, Fe II, Sc II, Ba II, Ti II) have developed, and in particular broad (FWHM ~ 700 km s $^{-1}$) from the UV Ca II H&K lines. Medium- and high-resolution spectra reveal a counter-P Cygni absorption profile in H α . Finally, late time spectra show an orange continuum ($T \sim 4000 - 5000$ K), a return in strength of the Balmer lines and the formation of molecular absorption bands. AT 2025abao is the rare case of a LRN with detailed archival information regarding the progenitor system. For the first time, we obtained the spectral energy distribution in the infrared of the precursor of a LRN, which is consistent with that of an M giant/AGB. We propose that the dichotomy of light curve behaviour in LRNe (two peaks vs. plateau) can be explained by the extent and H-richness of the common envelope.

Key words. supernovae: individual: AT 2025abao, galaxies: individual: M 31

1. Introduction

Luminous Red Novae (LRNe; [Kulkarni et al. 2007](#)) are astrophysical transients likely resulting from the coalescence of two non-degenerate stars due to the loss of systemic angular momentum following the ejection of a common envelope (e.g., [Tylenda et al. 2011](#); [Ivanova et al. 2013b,a](#); [Kochanek et al. 2014](#); [Pejcha 2014](#); [MacLeod et al. 2022](#)). They are a subclass of “interacting gap transients” (IGTs; [Pastorello & Fraser 2019](#); [Cai et al. 2022a](#); [Reguitti et al. 2026](#)). IGTs have absolute magnitudes at maximum in the range $-15 \lesssim M_V \lesssim -10$ mag, and fill the observational gap that separates the brightest novae from the faintest supernovae. In addition, their photometric and spectroscopic evolution is dominated by the effects of the interaction with a circumstellar medium (CSM, see [Pastorello et al. 2019a](#) for a review on the phenomenon).

LRNe are identified through a few recurrent observational characteristics. Firstly, they present a light curve with a double peak. The first peak has a short duration (~ 1 week); it is typically very luminous and characterised by a blue colour. This first maximum is followed a few weeks (or even months) later by a long-lasting second peak or a plateau-like phase, which is redder and usually fainter than the first¹.

The spectra of LRNe show a remarkable evolution, with three main phases: at the time of the first peak, the spectra display a blue continuum with narrow Balmer emission lines, similar to those of SNe IIn ([Fraser 2020](#)). At the second peak, which

sometimes is more akin to a plateau, the continuum cools to that of a yellow/orange star (~ 5000 -6000 K). At this phase, the Balmer lines become very weak, while a forest of absorption lines from neutral and singly-ionized metals (such as O, Ca, Fe, Sc, Ba, V, Ti) dominate the spectrum. Finally, in the third stage - after the second peak - the spectral continuum changes again to resemble that of a red giant star, with a photospheric temperature of only 3000-4000 K. On top of it, the narrow H α line in emission becomes prominent again, whereas molecular absorption bands from VO and TiO devour the continuum.

For a number of extragalactic LRNe, the progenitor systems were detected in pre-outburst archival images from deep ground-based facilities or space telescopes ([Fraser et al. 2011](#); [Mauerhan et al. 2015](#); [Smith et al. 2016](#); [Blagorodnova et al. 2017](#); [Cai et al. 2019](#); [Pastorello et al. 2021c](#); [Blagorodnova et al. 2021](#); [Cai et al. 2022b](#)). From these findings, it was discovered that the typical progenitors of LRNe are yellow hypergiant stars, with masses up to $50 M_\odot$ ([Guidolin et al. 2026](#)), and are suggested to sit in the Hertzsprung gap of the HR diagram ([Tranin et al. 2025](#); [Addison et al. 2022](#)).

Most LRNe are discovered in distant galaxies, hence they are usually faint targets, making challenging their observational campaigns and, consequently, limiting the amount of information we can infer from their study. For this reason, it is important to find and study IGTs in nearby galaxies, especially within the Local Group. A handful of LRNe were observed in the Milky Way: V4332 Sgr ([Martini et al. 1999](#); [Tylenda et al. 2005](#)), OGLE-2002-BLG360 ([Tylenda et al. 2013](#)), V838 Mon ([Munari et al. 2002](#); [Bond et al. 2003](#); [Tylenda 2005](#)), and V1309 Sco ([Mason et al. 2010](#); [Tylenda et al. 2011](#)). Three others were instead observed in M 31: M31-RV ([Mould et al. 1990](#); [Boschi &](#)

* E-mail: andrea.reguitti@inaf.it

¹ However, see the case of AT 2011kp (a.k.a. NGC4490-OT2011; [Pastorello et al. 2019a](#); [Smith et al. 2016](#)), which had a second peak that was more luminous than the first one.

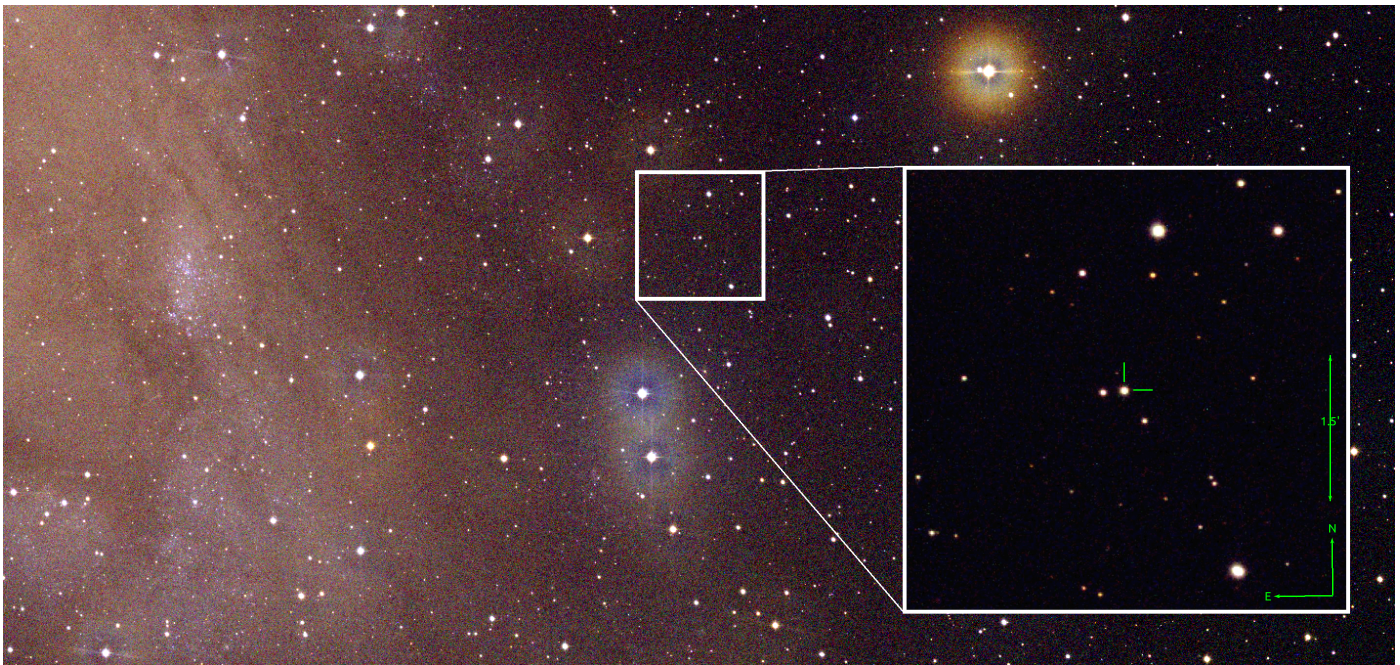


Fig. 1. Finding chart of AT 2025abao. The colour image is a composition of B , V , and r frames obtained by the Asiago 67/92cm Schmidt telescope on 7 November 2025, at the time of the maximum light. The spiral disk of M 31 is visible towards the left edge of the frame. The transient location is highlighted in the zoom-in panel to the right. Scale and orientation are reported.

Munari 2004), M31-LRN2015, (Kurtenkov et al. 2015; Williams et al. 2015; MacLeod et al. 2017; Lipunov et al. 2017; Blagorodnova et al. 2020), and AT 2019zhd (Pastorello et al. 2021a).

In this work, we present the results of our follow-up campaign of AT 2025abao, the fourth event of its type discovered in the Andromeda Galaxy. The proximity of M 31 (only 750 kpc away) allows us to constrain the progenitor parameters, and to provide a rich dataset of the transient event in terms of cadence, time coverage, resolution, and signal. Another paper was published illustrating the pre-outburst evolution of the source that later generated LRN AT 2025abao (labelled with the survey names WNTR23bzdiq and WTP19aalzlk; Karambelkar et al. 2025b, hereafter K25), and predicting a later evolution towards a LRN. In particular, the discovery of AT 2025abao offered the rare opportunity to perform a detailed analysis of its progenitor system in a stage of relative quiescence, and to study in detail its spectro-photometric properties a short time before the outburst onset². Through the analysis of infrared data, K25 infer that the progenitor of AT 2025abao was an early asymptotic giant branch (AGB) star with a temperature of about 3,500 K, a luminosity of $1.6 \times 10^4 L_{\odot}$, a radius of $350 R_{\odot}$, and a mass of $7 \pm 2 M_{\odot}$. Over a period of about seven years before the LRN outburst, the star increased its luminosity by a factor of three, with a limited colour/temperature evolution, while the spectrum showed properties compatible with those of an M-type star. The global (though slow) luminosity rise of the source was accompanied by fluctuations in its light curve, compatible with the presence of a binary companion. K25 suggested that the stellar brightening was the consequence of the common envelope evolution of a binary system having an AGB star as a primary member. Our paper will analyse the later evolution on the object, from the late pre-LRN phases to the LRN outburst.

The structure of the paper is the following: in Section 2 we present the discovery circumstances of AT 2025abao, and some

observational characteristics. The photometric dataset and the light-curve evolution are presented in Section 3, where the transient is also compared to other LRNe objects with similar properties. The spectral sequence is shown and analysed in Section 4, and finally the results are discussed in Section 5.

2. Discovery

AT 2025abao was officially discovered on 2025 October 19.8196³ (Modified Julian Date, or MJD = 60967.8196) by the Mobile Astronomical System of Telescope-Robots program (Kechin et al. 2025), at an unfiltered magnitude of 17.3 (Vega mag), and immediately reported to the Transient Name Server⁴ (TNS). However, the first advisory of a brightening from a known transient was made by Koichi Itagaki on October 17.4798, at an unfiltered magnitude of 17.8 (Vegamag)⁵. An even earlier pre-discovery measurement was provided by Fabregat et al. (2025) on October 14. The LRN appeared in the south-west quadrant of the very nearby Andromeda galaxy (M 31), at celestial coordinates $\alpha = 00:38:48.62$, $\delta = +40:46:07.6$ (45' West and 30' South of the nucleus), in the outskirts of its spiral disk. The location of the transient is shown in Figure 1. AT 2025abao was correctly classified on 2025 November 2 as a LRN by Taguchi & Maeda (2025b), who noted similarities with another LRN found in M 31, AT 2019zhd (Pastorello et al. 2021a). For the distance to M 31, we assume the same value adopted by Pastorello et al. (2021a) ($\mu = 24.47 \pm 0.06$ mag, $d = 0.785$ Mpc). Its redshift is $z = -0.001$ (Falco et al. 1999). However, we note that the peaks of the spectral lines of AT 2025abao are blueshifted by $z = -0.0015$. The additional radial velocity is likely caused by the rotation curve of the galaxy disk, with the object being located on the side approaching us at ~ 150 km s⁻¹ (Chemin et al. 2009). The Galactic reddening towards AT 2025abao is modest,

³ Universal Time is used throughout the paper.

⁴ <https://www.wis-tns.org/>

⁵ <http://www.cbat.eps.harvard.edu/unconf/followups/J00384865+4046079.html>

although not negligible, $A_V = 0.17$ mag (Schlafly & Finkbeiner 2011). Given the peripheral location of AT 2025abao in the disk of M 31, additional contribution to the dust extinction is likely negligible. Hereafter, in agreement with K25, we will only account for the dust attenuation within the Milky Way.

3. Photometric evolution of AT 2025abao

3.1. Observations and data reduction

While K25 presented early photometric data of AT 2025abao, this work complements their light curve with previously unpublished pre-LRN photometric points from the Zwicky Transient Factory (ZTF; Bellm et al. 2019; Graham et al. 2019). The initial phases following the LRN outburst were exclusively monitored by amateur astronomers and all-sky surveys, such as ZTF and the Asteroid Terrestrial-impact Last Alert System (ATLAS; Tony et al. 2018). Our multi-band optical and near-infrared (NIR) follow-up campaign began shortly after the spectroscopic classification of the object, and lasted for approximately three months. The *Swift* space telescope was also triggered to get ultraviolet (UV) photometry at early phases. The facilities used to collect our photometric data are listed in Table C.1. The photometric data were reduced using standard procedures with the dedicated ECsnoopy pipeline⁶. Instrumental magnitudes were determined through the Point Spread Function (PSF)-fitting technique, and calibrated against the catalogue of the Sloan Digital Sky Survey (SDSS) survey (Ahumada et al. 2020). The *Swift*/UVOT UV data were reduced with the HEASOFT pipeline v. 6.35.2⁷, by aperture photometry within a fixed radius of 5''. We also retrieved calibrated forced photometry measurements from the ALeRCE Broker (Förster et al. 2021) for ZTF, and from the public Forced Photometry server⁸ (Shingles et al. 2021) for ATLAS. Given its apparent brightness, the object was also observed extensively by amateur astronomers⁹; the magnitudes were measured via aperture photometry on their pre-reduced frames (corrected for bias, flat-field, and dark frames), and calibrated their measurements against the AAVSO Photometric All-Sky Survey¹⁰ catalogue (Henden 2019). The final UV, optical (Sloan, Johnson, and ATLAS), and NIR magnitudes are listed in the CDS, while the light curves are plotted in Fig. 2.

3.2. Light Curve of AT 2025abao, and its interpretation

3.2.1. Pre-outburst phase

The photometric evolution of the transient during the pre-LRN was extensively studied by K25. The light curve of the transient experienced a slow, long-lasting (about seven years) brightening, with some luminosity fluctuations superposed on that global trend. Additional photometric points presented in this paper show that the source reached a relative maximum about one year before the LRN discovery, followed by a poorly-sampled luminosity decline to a pre-outburst minimum (see, also, Sect. 3.4).

⁶ ECsnoopy is a package for SN photometry using PSF fitting and/or template subtraction developed by E. Cappellaro. A package description can be found at <https://sngroup.oapd.inaf.it/ecsnoopy.html>.

⁷ NASA High Energy Astrophysics Science Archive Research Center – Heasarc 2014.

⁸ <https://fallingstar-data.com/forcedphot/>

⁹ More observations of AT 2025abao during the outburst are presented by Mikolajczyk et al. (2026).

¹⁰ <https://www.aavso.org/apass>

The pre-outburst evolution of AT 2025abao, from the slow luminosity rise to a broad peak, the superposed magnitude fluctuations, and the following luminosity decline, closely resembles that observed in V1309 Sco (Tylenda et al. 2011). In both cases, the peculiar light-curve evolution is likely a consequence of unstable mass transfer between the stellar components of a binary system (Roche Lobe overflow; see, e.g., Pejcha 2014; Pejcha et al. 2016b). This culminates with the formation of a common envelope embedding the stellar system which becomes progressively optically thick (Ivanova et al. 2013b). A slow pre-LRN luminosity rise was also observed in other LRNe discovered in M 31, such as M31-LRN-2015 (Blagorodnova et al. 2020) and AT 2019zhd (Pastorello et al. 2021b), as well as in several extragalactic LRNe, although with some limitations due to a lower monitoring cadence and the poorer signal-to-noise datasets¹¹.

3.2.2. LRN outburst

In the case of AT 2025abao, this phase is followed by a fast brightening of about five magnitudes in the r -band (six in g): this is the onset of the LRN outburst. The rapid rise lasts about one week from the discovery of AT 2025abao. Then, its light curve settles on a sort of plateau phase during which the object maintains a nearly constant brightness ($V \simeq 14.9$ mag). To constrain the timing of the main LRN maximum, we perform a 2nd-order polynomial fit to the g -band data collected between MJD = 60973 and MJD = 61000, determining that the light curve peaked on MJD 60986.3 ± 0.2 , at a magnitude of $g = 15.10 \pm 0.02$ mag. This epoch will be used as a reference for all phases considered in this paper. We note that the bluer-band light curves peak earlier (-2.7 d in u , -1.4 d in B), while a photometric peak is not well-defined in the red bands, where a plateau is noticeable, lasting for about two months. This plateau is followed by a sudden decline of the light curve. We measured the post-maximum decline rates in the optical bands by fitting the light curve in each filter with a straight line. The decline is steepest in the u -band (3.9 ± 0.2 mag 100 d $^{-1}$), and less and less steep as we move towards redder filters ($\gamma_B = 2.8 \pm 0.1$, $\gamma_g = 1.5 \pm 0.1$, $\gamma_V = 0.29 \pm 0.03$ mag 100 d $^{-1}$). The r -band light curve instead is flat, and the i -band one is actually still rising, up to phase +45 d, when it reached its maximum.

Individual patterns of LRN light curves are not fully understood. However, there is a general consensus that the characteristic double-peaked shape is due to a merging event. As a consequence of the common envelope ejection and the loss of systemic angular momentum, the two components of the binary system may merge. If this happens, the main LRN outburst is produced by the violent ejection of material following the coalescence of the two stellar cores, and its subsequent interaction with the pre-existing common envelope (see, e.g., Metzger & Pejcha 2017; MacLeod et al. 2017, 2022; Matsumoto & Metzger 2022; Kirillov et al. 2025).

3.3. Colour evolution

The intrinsic colours of AT 2025abao, blue soon after its discovery ($B - V = 0.45$ mag at -4 d), evolve to redder colours after the

¹¹ The slow brightenings heralding LRN eruptions were observed for AT 2014ib (SNhunt248; Kankare et al. 2015; Mauerhan et al. 2015), AT 2015dl (M101-2015OT1; Blagorodnova et al. 2017; Goranskij et al. 2016), AT 2020hat (Pastorello et al. 2021c; Reguitti et al. 2026), AT 2021blu (Pastorello et al. 2023) and, more marginally, in AT 2011kp (Pastorello et al. 2019b) and AT 2021biy (Cai et al. 2022b).

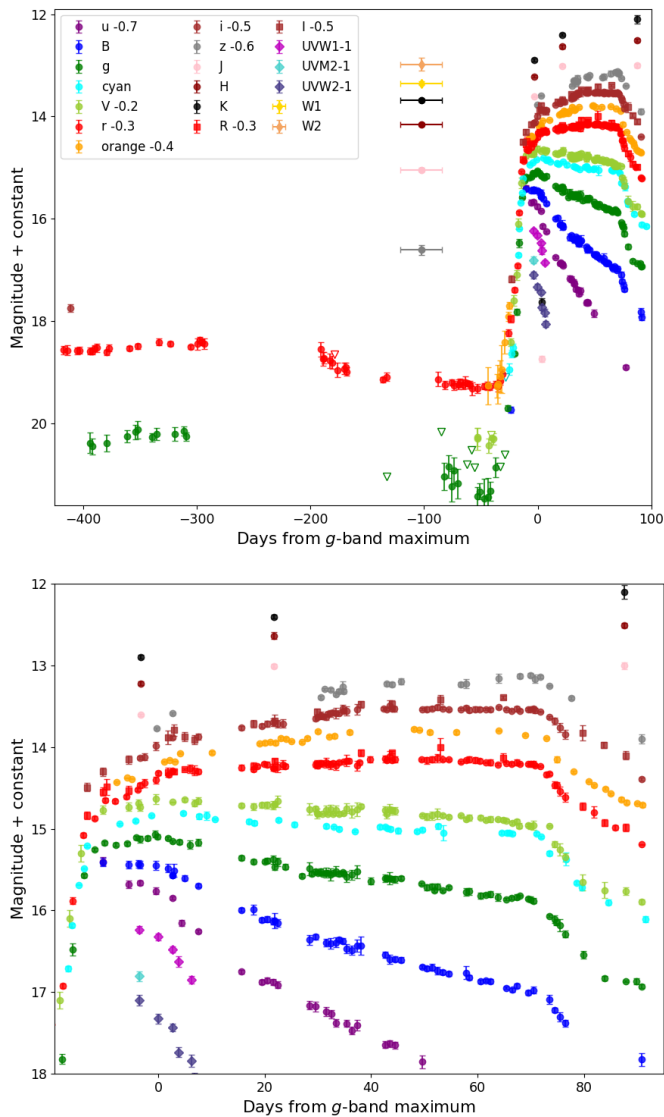


Fig. 2. Optical light curves of AT 2025abao. Top panel: the entire evolution since October 2024, when the follow-up campaign of WNTR23bzdiq conducted by K25 ended. The pre-LRN light curve, its decline to the minimum, and the final rapid rise to the LRN peak are visible. Bottom panel: zoom in on the fast rise towards the maximum light, the 70 days-long plateau, and the fall from it.

V-band maximum ($B - V = 0.8$ mag at +8 d, $B - V = 1.0$ mag at +15 d). Thanks to the scanning by the ZTF survey we have, for the first time, an indication of the optical colour of a LRN during the pre-outburst slow luminosity rise. The $g - r$ colour stays roughly around 1.4 mag one year before the g -band maximum. Then, it reaches a maximum up to ≈ 1.7 mag (with large scatter) at the time of the r -band minimum (−2 months). $g - r$ decreases to 1.1 mag at −30 d, at the start of the fast rise to the first peak, diminishing to a lowest of +0.0 mag at −12 d. From there, $g - r$ increases again to 1.3 mag at +76 d, at the time of the plateau drop. The colour curves of AT 2025abao are shown in Figure 3.

3.4. Comparisons with similar objects

As comparison objects, we select a few faint LRNe well monitored during the slow pre-outburst rise phase. Given that AT 2025abao has an extensive and well-sampled light curve

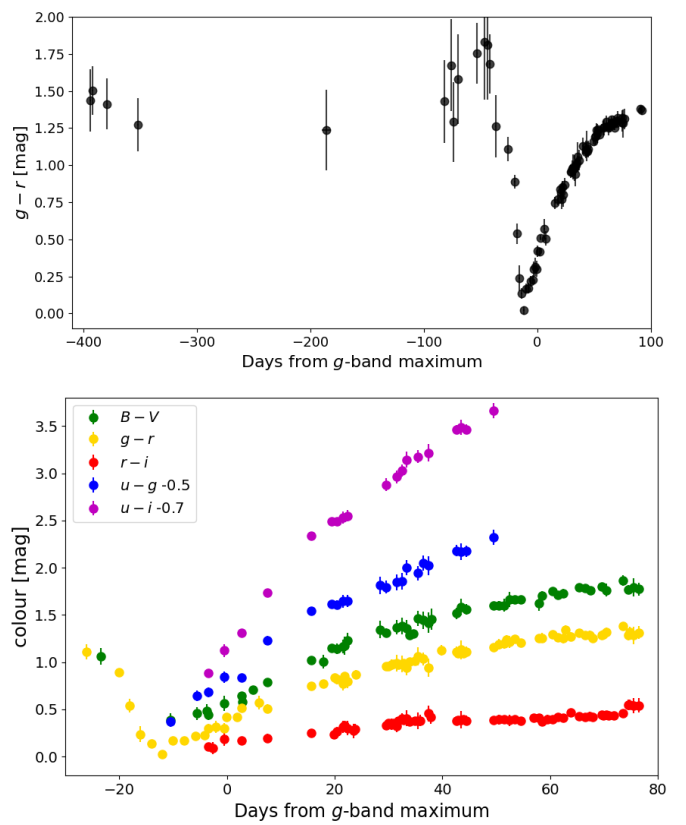


Fig. 3. Colour curves of AT 2025abao. Top panel: Evolution of the $g - r$ colour from −1.1 yr to +3 months. The colour changes prominently between the slow pre-outburst rise and optically thick phase, the fast rise and the first peak. Bottom panel: Evolution of multiple colour curves ($B - V$, $g - r$, $r - i$, $u - g$, $u - i$) around the maximum light and plateau.

since a few years before the LRN event (K25), our primary reference object is V1309 Sco (Mason et al. 2010; Tytla et al. 2011), although the two objects have significantly different light curves during the outburst. AT 2025abao reaches an absolute magnitude at the r -band peak of $M_r = -10.2 \pm 0.1$ mag (Fig. 4), hence it lies at the faint edge of the extragalactic LRNe brightness distribution, although it is significantly more luminous than Galactic objects such as V1309 Sco and V4332 Sgr (Pastorello et al. 2019a). AT 2019zhd (in M 31; Pastorello et al. 2021a) and the Galactic V838 Mon (Goranskij et al. 2020, and references therein) have similar absolute magnitude at maximum as AT 2025abao, and are hence selected as comparison objects.

As mentioned in Sect. 3.2.1, the pre-outburst light curves of both AT 2025abao and V1309 Sco were very well monitored (see Fig. 4). While the former was much brighter at the top of the slowly rising phase (about one year before the LRN outburst onset), reaching $M_r \sim -6$ mag, the latter reached only $M_I \sim +3$ mag. Then, both objects dimmed towards the optically thick common envelope phase. In particular, AT 2025abao reached a minimum at $M_r = -5.0$ mag at −42 d, before starting the fast rise towards the LRN maximum light, when it increased its brightness by about 6 mag.

From the comparison in Fig. 4, we note that the fast rise of AT 2025abao to the main peak is very similar to that exhibited by AT 2019zhd, in both speed and luminosity. At peak, the absolute magnitude of AT 2025abao in the r band is only marginally brighter than those of AT 2019zhd ($M_r = -9.6$ mag) and V838 Mon ($M_R = -9.9$ mag; note that the Figure shows the

V-band light curve, which peaks at $M_V = -9.6$ mag). Then, its light curve shows a flat, long-lasting (about two months) plateau, while the comparison objects show a short-duration (less than a week) early peak before declining. V838 Mon shows a more structured post-maximum light curve, with a later rebrightening (e.g., [Munari et al. 2002](#)). In contrast to the comparison objects, the outburst of V1309 Sco is much fainter, and a shift upwards by 2.5 mag has to be applied to its I -band absolute light curve in Fig. 4 to match the peak luminosity of AT 2025abao.

Due to the plateau-like feature after the first peak, the light curve of AT 2025abao is reminiscent of other LRNe that do not exhibit an evident second red peak, instead showing a long phase of nearly constant luminosity. Known LRNe with plateau-like light curves are AT 2021afy ([Pastorello et al. 2023](#)), although it is 4.5 mag more luminous and at the bright edge of the LRNe brightness distribution; AT 2018bwo, whose plateau reaches $M_r = -10.8$ mag ([Blagorodnova et al. 2021; Pastorello et al. 2023](#)); AT 2020hat, that peaks at $M_r = -11$ mag ([Pastorello et al. 2021c](#)). However, we remark that AT 2018bwo was discovered already after the first peak due to the Solar conjunction, hence the object could have reached a higher peak luminosity.

3.5. Bolometric light curve

Given that only some photometric bands are available before the discovery and the start of the follow-up campaign of the main outburst, we divided the dataset in two parts and constructed two different bolometric light curves: (1) We first constructed a pseudo-bolometric curve selecting only the g, c, V, r, o, I bands, integrating their fluxes (inferred by converting the magnitudes taking into account for the distance and reddening) with the trapezoidal rule from -50 to -3.5 days, hence covering the pre-discovery phases. (2) Then, we built the bolometric curve of AT 2025abao extended from the UV to the NIR, accounting for the contribution from $UVW2$ to K bands, starting at the discovery epoch, hence covering only the main LRN outburst. For epochs without observations in some bands, we interpolated the available data using the r -band light curve as a reference and assuming a constant colour index. Both the pseudo- and the fully bolometric curves of AT 2025abao are shown in Fig. 5.

The bolometric luminosity of AT 2025abao at the time of the g -band maximum is $\log_{10}(L_{\text{bol}}/\text{erg s}^{-1}) = 39.45 \pm 0.03$, similar to the values reached by the comparison objects. However, its top luminosity ($\log_{10}(L_{\text{bol}}/\text{erg s}^{-1}) = 39.52 \pm 0.03$) is reached about 67 d later, just before the fall from the plateau. This peak bolometric luminosity makes AT 2025abao the brightest LRN ever discovered in M 31 and, at the time of the peak, one of the most luminous objects within that galaxy. However, while the bolometric luminosity of AT 2025abao at peak is similar to that of the comparison objects and the fast rise resembles that of AT 2019zhd, the later evolution is completely different, as none of the LRNe considered presents a 70 d-lasting plateau. In this respect, AT 2025abao is more similar to AT 2018bwo ([Blagorodnova et al. 2021; Pastorello et al. 2023](#)), although the former is about three times fainter.

3.6. SED evolution

We constructed the Spectral Energy Distribution (SED) of AT 2025abao at different epochs, starting from phase -3.5 d, combining the photometric data from the NUV to the NIR domains. Then, we fitted them with a Planckian function to estimate how the black-body (BB) temperature (T_{BB}) and the radius

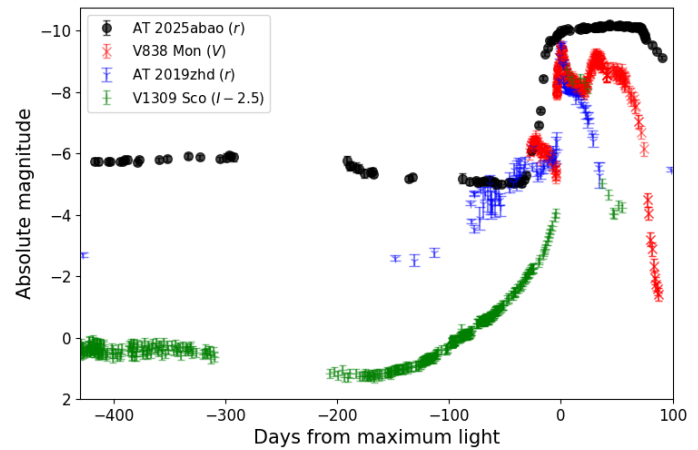


Fig. 4. Absolute light curve of AT 2025abao in the r band, compared with those of AT 2019zhd (r -band), V838 Mon (V -band), and V1309 Sco (I -band). The light curve of V1309 Sco is scaled upwards by 2.5 magnitudes to match the peak brightness, and to see the pre-outburst slow rise of both V1309 Sco and AT 2025abao. The error bar on the distance modulus of V1309 Sco (0.724 mag) is not shown.

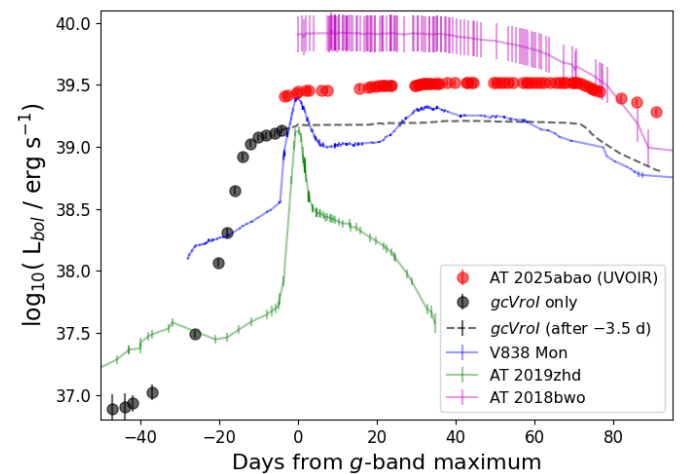


Fig. 5. Pseudo-bolometric (just g, c, V, r, o, I bands) light curve of AT 2025abao, in black, and UV+Optical+NIR ($UVW2$ to K bands) bolometric curve of the main outburst, in red. The separation is made at phase -3.5 d, when our multi-band photometric follow-up campaign started (after this phase, the $gcVrol$ pseudo-bolometric is shown as a dashed line). While the bolometric luminosity of AT 2025abao was similar at the time of the g -band maximum to those of the comparison objects, the subsequent evolution is different.

(R_{BB}) evolve with time. Between -15 d and -3.5 d, we did so using only the data from the filters from u to I . For epochs without the photometric information in some filter, we made interpolations or extrapolations from adjacent epochs with available data, assuming no colour changes. The highest temperature was reached on -12 d (the epoch of the minimum $g - r$ colour), at $T_{\text{BB}} = 7100 \pm 300$ K. At the time of the g -band maximum light (see Fig. 6), the SED peaks at around 5000 Å and is fitted with a single BB function having a temperature of 5740 ± 140 K. The inferred photospheric radius is $870 \pm 50 R_{\odot}$. At these early phases, no IR excess is detected. In Fig. 7, we plot the temporal evolution of T_{BB} , R_{BB} , and the BB luminosity L_{BB} . During the plateau phase, the temperature slowly decreases and flattens at $T_{\text{BB}} \approx 4300$ K, slightly lower than that expected for the H recombination, as evidenced also by the redder shape of the spectral

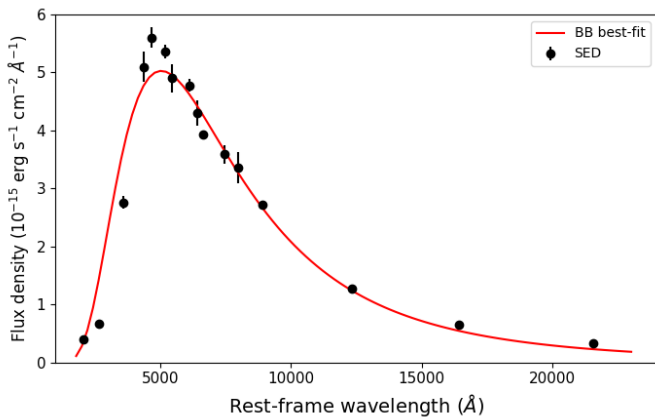


Fig. 6. SED of AT 2025abao at the epoch of the g -band maximum, together with the BB best-fit. A single Planckian function is sufficient to obtain a good match. Its parameters are $T_{\text{BB}} = 5740 \pm 140$ K and $R_{\text{BB}} = 870 \pm 50 R_{\odot}$.

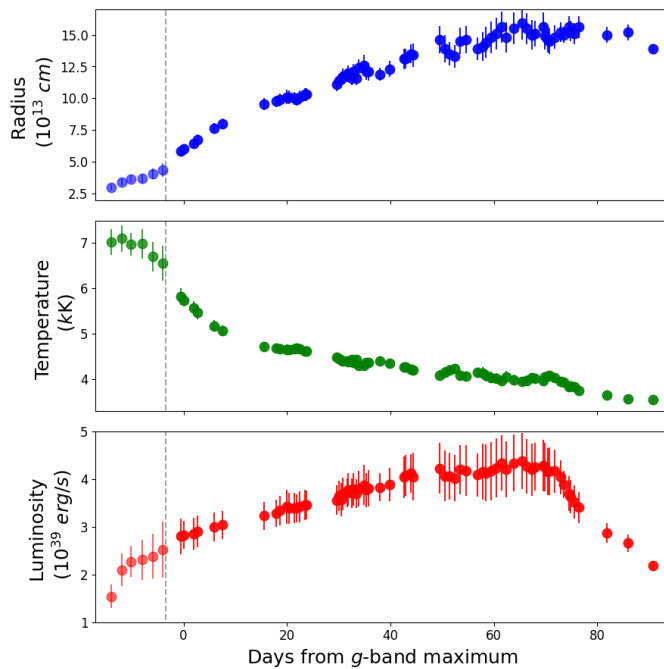


Fig. 7. Evolution of the BB radius, temperature, and luminosity of AT 2025abao starting from phase -15 d. Before -3.5 d (epoch marked by the gray dashed line) the parameters are determined based on only the filters between u and I , and afterwards they are estimated from the UV to the NIR coverage.

continuum in this phase (see Sect. 4). The photospheric radius when the object was hottest is $(3.4 \pm 0.3) \times 10^{13}$ cm (corresponding to $500 \pm 40 R_{\odot}$), while during the plateau phase it slowly expands to $\sim (15 \pm 1) \times 10^{13}$ cm (hence, $2150 \pm 140 R_{\odot}$). During the plateau phase, L_{BB} slightly increases from 3×10^{39} at the time of the g -band maximum to 4×10^{39} erg s^{-1} about 70 d later, before a sharp decrease after the fall from the plateau.

3.7. SPHEREx SED of the precursor

The Spectro-Photometer for the History of the Universe, Epoch of Reionization and Ices Explorer (SPHEREx; Bock et al. 2025) is a space telescope launched on 11 March 2025 to conduct an

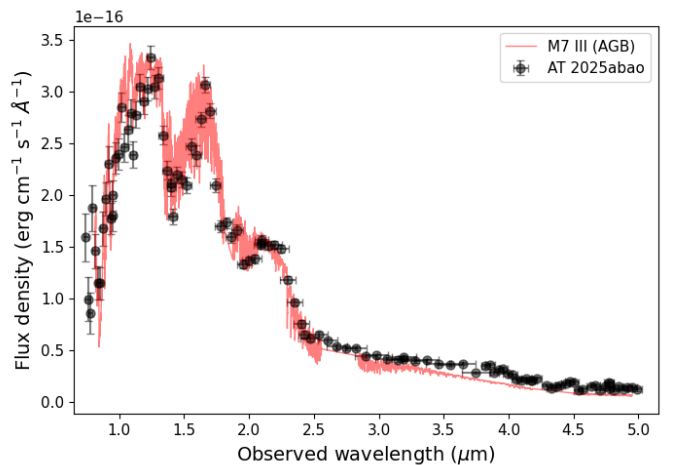


Fig. 8. Infrared spectral energy distribution of the precursor of AT 2025abao between 0.74 and 5.0 μm as obtained by SPHEREx 3–4 months before the g -band maximum light. Overplotted is a spectrum of an M7e III/AGB star.

all-sky survey in 102 infrared colours between 0.75 and 5 μm , hence covering a wide range of wavelengths from the NIR to the mid infrared (MIR) domains. During its first scanning of the whole celestial sphere, between MJD 60865 and 60902 (-121 d to -84 d), it observed the field of AT 2025abao during the pre-LRN phase, at a time close to the optical minimum. We retrieved the calibrated SED (Akeson et al. 2025; Hui et al. 2026), from the Spectrophotometry Tool available in the NASA/IPAC Infrared Science Archive webpage¹². The IR SED of the precursor of AT 2025abao from SPHEREx is presented in Figure 8.

This provides a rare opportunity to analyse a NIR/MIR spectrum of a precursor of an LRN, and probably for the first time, the MIR region is observed in spectroscopy. The source is faint in the bluest bands and shows a red continuum between 0.74 and $1.2 \mu\text{m}$. Three peaks are clearly present at 1.3 , 1.7 , and $2.2 \mu\text{m}$. These peaks, and the broad absorptions in between due to molecular absorption bands from TiO, H₂O, and CO, are also visible in the NIR spectra presented by K25 and taken in 2024 (see their Figure 3). Then, at $\lambda > 2.5 \mu\text{m}$, the SED is nearly flat in the MIR, which could be due to thermal emission from dust surrounding the progenitor system of AT 2025abao. For reference, in Fig. 8 we plot together a NIR/MIR spectrum of a M7e III star (HD 108849, a known AGB¹³) from the Atlas by Rayner et al. (2009), which perfectly matches the SED from SPHEREx. A modelling of the SED is presented in Sect. 5. Finally, we performed spectro-photometry on the SED to derive approximate NIR and MIR magnitudes (in z , J , H , K , WISE $W1$ and $W2$ bands) of AT 2025abao 3–4 months before the g -band maximum. The infrared colours are larger, hence redder, than during the outburst (for instance, $J - K = 1.36 \pm 0.05$ mag vs. 0.61 ± 0.03 mag at $+22$ d).

4. Spectral evolution

AT 2025abao was classified as a LRN on 2025 October 29, 10 days after the official discovery date and at a phase of -8.7 d

¹² <https://irsa.ipac.caltech.edu/applications/spherex/tool-spectrophotometry>

¹³ <https://simbad.u-strasbg.fr/simbad/sim-basic?Ident=bk+vir>

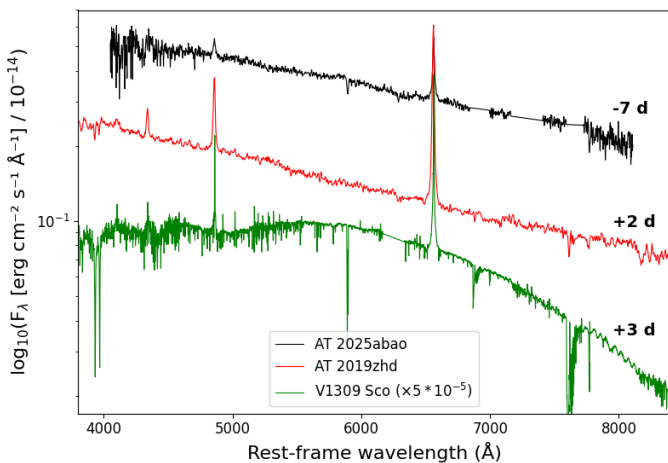


Fig. 9. Comparison of the earliest spectrum of AT 2025abao to the early spectra of the comparison objects AT 2019zhd and V1309 Sco (Mason et al. 2010). All objects show a hot, blue continuum with narrow emissions from H α and H β lines. At this early phase, V1309 Sco already presents signs of metal absorptions.

(Taguchi & Maeda 2025a). However, earlier spectra from amateur astronomers are also available. The earliest, taken on 2025 October 27 (phase -10.4 d), was presented by Skopal et al. (2025). One day later, another low-resolution spectrum was obtained by C. Balcon (phase -9.4 d), and additional spectra were obtained with a nearly daily cadence (at phases -6.6 , -5.3 and -4.4 d) by Taguchi & Maeda (2025a) and Skopal et al. (2025). These early spectra exhibit a blue continuum ($T_{\text{BB}} = 7100$ K) with superimposed narrow emission lines of the Balmer series, a feature typical of LRNe during the rise to maximum light (Pastorello et al. 2019b). The classification spectrum of Taguchi & Maeda (2025a), retrieved from the TNS, is shown in Fig. 9, where it is compared with spectra of LRNe AT 2019zhd and V1309 Sco at the maximum light to emphasize their overall similarity. Nonetheless, the spectral evolution of V1309 Sco is more rapid, and metal lines are already visible in absorption at these early epochs.

We conducted a spectroscopic follow-up of AT 2025abao, during which we collected 20 optical spectra spanning three months of evolution. The log of spectroscopic observations is given in Table C.2, and the spectral time series is shown in Figure 10, left panel. The spectra from the 1.22m Galileo telescope equipped with a Boller & Chivens (B&C) spectrograph and the 1.82m Copernico telescope with an Echelle spectrograph were reduced with a custom-made, IRAF-based pipeline developed by A. Siviero, while the spectra from the 2.56m Nordic Optical Telescope (NOT) with ALFOSC, the 1.82m Copernico telescope with AFOSC, and the 10.4m Gran Telescopio Canarias (GTC) plus OSIRIS were reduced using the fosogui¹⁴ pipeline. Finally, the spectra of the 3.58m Telescopio Nazionale Galileo (TNG) plus DOLORES spectra were hand-reduced using routine IRAF procedures.

On 2025 November 3 (phase = -3.4 d), we obtained a high-resolution ($R \sim 20,000$) Echelle spectrum with the Copernico 1.82-m telescope, in which we can identify specific spectral features. The main spectral features identified in this spectrum are highlighted in Fig. 11. H α and H β have a narrow P Cygni absorption

profile on top of a much broader component, with a velocity of 40 km s^{-1} (Figure 11, right panel). Along with the H lines, we clearly identify prominent Na I D doublet features, all the components well discerned. However, while the absorption lines of the Na I D doublet at redshift zero are unresolved and hence can be attributed to material along the line of sight within the Milky Way, the Na I D doublet lines at the redshift of M 31 are resolved, and have a FWHM of around $20\text{--}25 \text{ km s}^{-1}$ (see Fig. A.1 in Appendix A, top panel). This FWHM velocity is similar to those exhibited by other metal lines visible already in the -3.4 d spectrum (see below), hence we consider these Na I D features as intrinsic to the transient. A prominent absorption feature is observed at 5890.9 \AA , which is unlikely to be an additional Na I component, and whose nature will be discussed in Appendix A. Lines of the Mg I triplet at $5160\text{--}5180 \text{ \AA}$ are also detected, with a FWHM velocity similar to that of the Na I D lines. More metal lines are detected bluewards of 5200 \AA , including from Fe II, which also have a FWHM velocity of 25 km s^{-1} . Finally, broad Ca II H&K absorption lines are visible in the UV region, with a much higher FWHM velocity of $\sim 600 \text{ km s}^{-1}$ (Figure 11, left panel), due to its opaqueness.

In the spectra taken at about the g -band maximum light, together with a double-horned H α line, a faint He I 6678 is the only other transition seen in emission, on top of a continuum peaking at $4800\text{--}4900 \text{ \AA}$ (indicating $T_{\text{BB}} \sim 6000$ K, consistent with the SED inferred in Sect. 3.6). Most notable features are the deep and strong absorptions of the Ca II H&K UV doublet, Na I D, and a forest of metal lines. In particular, the Fe II multiplet 42 ($\lambda\lambda\lambda 4924, 5018, 5169$) transitions are clearly detectable.

Already by the $+2.7$ d spectrum, the continuum temperature has declined to 5200 K (with the spectral continuum emission peaking at around 5600 \AA). The gas cooling is confirmed by the disappearance of the He I 6678 line. Otherwise, the spectrum did not change significantly, with the most prominent metal transitions still clearly present. In the $+9.7$ d spectrum, the continuum peaks at around 5900 \AA , indicating a temperature of only ~ 4900 K. Emission lines, including H α , have completely disappeared, and visible features are only in absorption. Multiple metal lines are identified in the bluer region, together with the usual Ca II (both H&K and IR triplet) and Na I D. Little has changed in the spectrum at $+16.7$ d. A broad basin is visible between 4800 and 5300 \AA , a feature commonly seen in the spectra of Sun-like stars, and attributed to the absorption due to the CH radical molecule.

In the $+24.7$ d spectrum, as already in the $+18.5$ d spectrum, the continuum peak has shifted to around 6800 \AA ($T \sim 4250$ K), maintaining a steep decline towards the UV likely due to line blanketing, while being flat at redder wavelengths. The strongest features are now the absorptions from the Ca II NIR triplet, though the Ca II H&K absorption lines are also recognizable, together with the depression due to CH, and even more numerous metal lines. Balmer lines are now weak or absent.

On December 10 (phase = $+33.6$ d), we took another Echelle spectrum, which reveals an astonishing peculiarity: the H α line presents a counter P Cygni profile, i.e. a narrow absorption redwards of the centre of the emission line. The velocity of the minimum of this feature indicates an infalling velocity of $\sim +70 \text{ km s}^{-1}$. The component is confirmed as it is detected also in the H β line (see Fig. 12, where its profile is overlapped with that of H α). This second Echelle spectrum also shows a crowded line population in the $5850\text{--}5900 \text{ \AA}$ region: a blueshifted He I $\lambda 5876$ emission line, two Na I D doublets (one due to line-of-sight material in the MW, and the other intrinsic to AT 2025abao), and

¹⁴ Fosogui is a graphic user interface aimed at extracting SN spectroscopy and photometry obtained with FOSC-like instruments. It was developed by E. Cappellaro. A package description can be found at <http://sngroup.oapd.inaf.it/fosogui.html>.

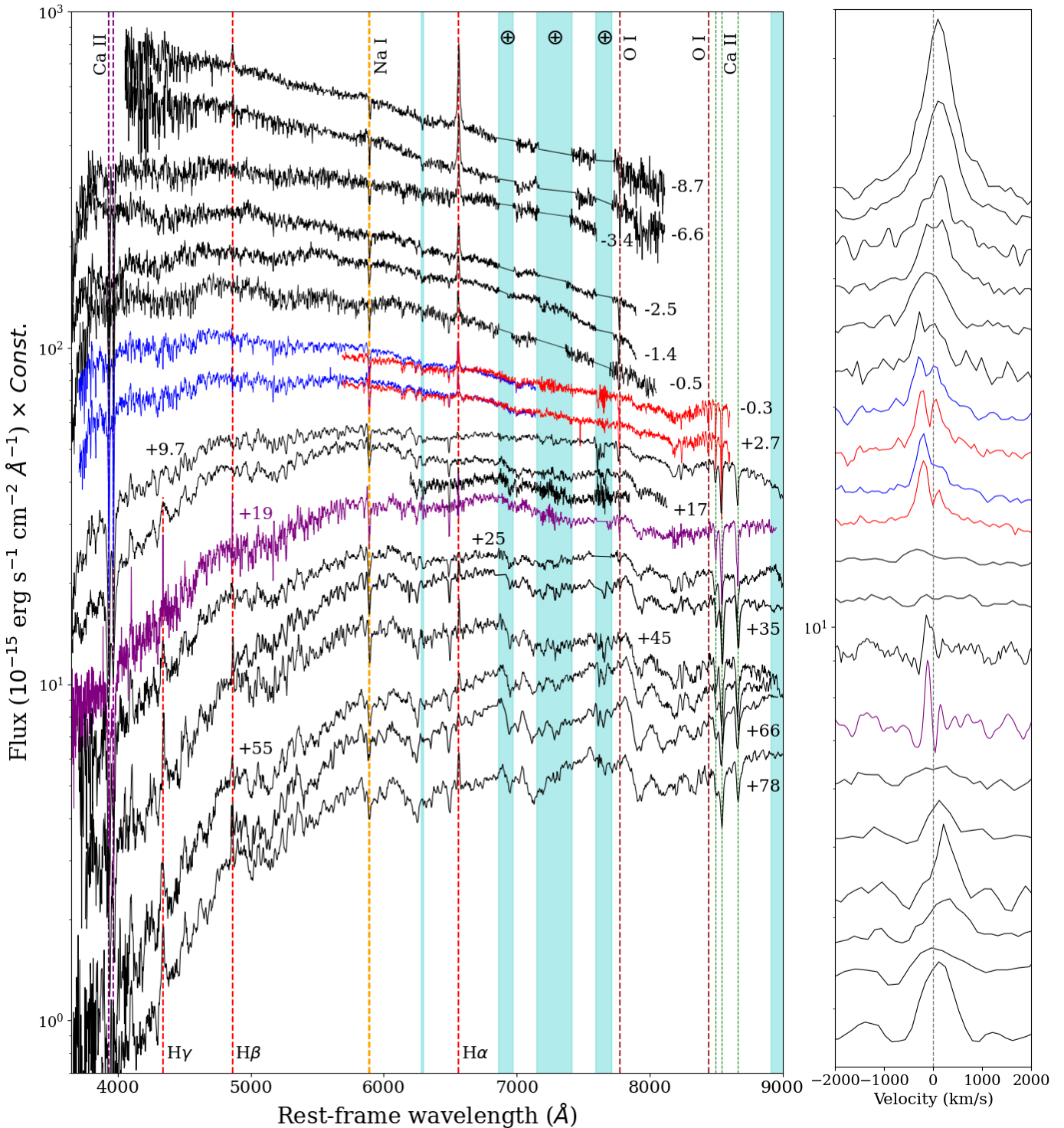


Fig. 10. Left: Spectral time series of AT 2025abao and basic line identification. The spectra are corrected for blueshift and total reddening, and are plotted in logarithmic scale. The mid-resolution GTC+OSIRIS spectrum is highlighted in purple, while the NOT+ALFOSC gr7 and gr8 spectra, taken on the same night, are shown in blue and red, respectively. Phases in days are reported in the right side of each spectrum. The regions contaminated by telluric absorptions are identified with cyan bands. Right: Evolution of the H α profile in the velocity space.

two more lines at $\lambda 5890.9$ and $\lambda 5896.9$, also discussed in Appendix A.

In the +45 d spectrum of AT 2025abao, the first signs of molecular absorption bands: TiO features start to appear between 6000 and 8000 \AA , in the form of two sawtooth drops in the continuum, sharp on the blue edge and then gradually ris-

ing towards the red edge. This trend of molecules formation is confirmed in the +66 d spectrum. Molecular bands from VO and TiO are clearly present in the regions 6100-6700 \AA and 7100-7800 \AA , together with a rise at the start of the NIR, in the range 8400-8800 \AA , also compatible with a molecular band. The continuum peaks at around 7800 \AA ($T \sim 3700$ K), with a temper-

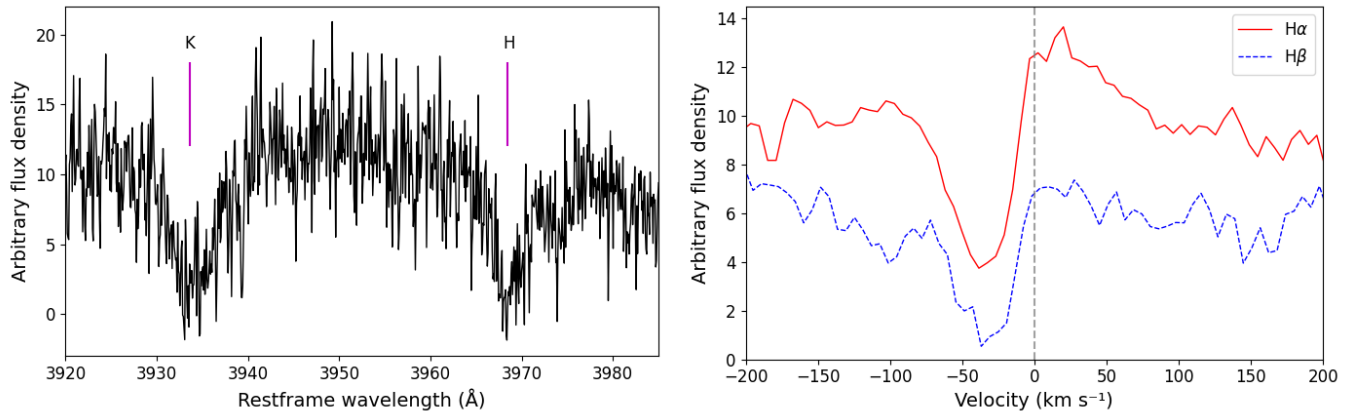


Fig. 11. Zoom in on some spectral lines visible in the -3.4 d Echelle spectrum. Left: Ca II H&K. Right: H α and H β , overlapped in the velocity space, with a P Cygni profile at -40 km s $^{-1}$ clearly visible.

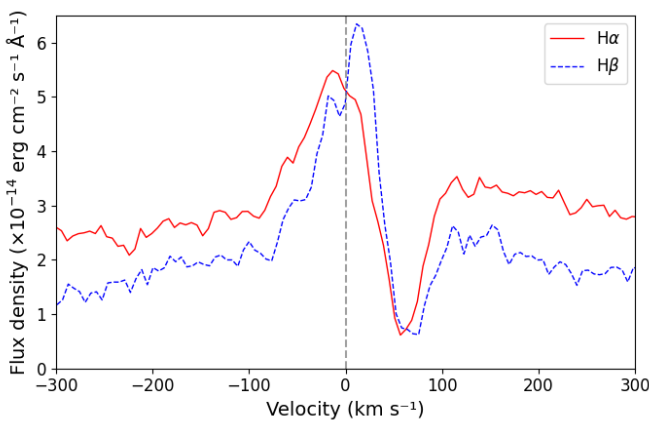


Fig. 12. Zoom on the H α and H β lines, in velocity space, in the $+34$ days Echelle spectrum, showing a counter P Cygni profile at $+70$ km s $^{-1}$.

ature trend consistent with that expected for a moderately faint LRN. Balmer lines appear to be strong again in the $+78$ d spectrum, while the continuum is now red and its temperature has decreased to 3600 K.

4.1. Spectral line identification

On November 25 ($+18.5$ d), four medium-resolution ($R \sim 2, 100$) spectra were obtained with 10.4m GTC+OSIRIS and the R2500-class grisms, covering wavelengths from the U to the I bands. In these spectra, we identified the most prominent metal lines, highlighting that these features are real and not noise patterns, since for each grism we took four exposures in sequence and checked whether a line was present in all individual spectra.

In the AT 2025abao spectrum, H α shows a narrow P Cygni profile with a dominant absorption with a minimum blue-shifted by -200 km s $^{-1}$, and a weaker and narrow emission component. However, on the red side, a sharper counter P Cygni is also present. This feature is common in LRN spectra (see AT 2011kp; Pastorello et al. 2019b), and can be interpreted as outflowing material from the central system through the second Lagrangian point (Pejcha et al. 2016a) in a direction opposite to the observer. Other Balmer lines are detected (H β , H γ , and H δ , and possibly also H ϵ), dominated by the emission component. Ca II H&K are relatively broad (FWHM = $800 - 1000$ km s $^{-1}$) and in pure

absorption. Other notable absorption features are the Ca II NIR triplet, and the Na I D doublet. All other features, while present and identified, are less strong.

In Fig. 13, we compare the full GTC+OSIRIS mid-resolution spectrum of AT 2025abao with that of AT 2011kp during late phases ($+103$ d) from Pastorello et al. (2019b), who also performed a similar line identification in a mid-resolution spectrum. The spectrum of AT 2025abao was taken 20 days after maximum, while that of AT 2011kp was obtained after more than three months. While the spectral continuum shows some differences, the most important metal lines are identified in both spectra. This is an indication of a much faster evolution of AT 2025abao. Thus, a similar set of lines is identified and visualized in both spectra: multiplets from Fe II, Fe I, Mg I, Sc II, Ba II (the strongest line being $\lambda 6497$) and Ti II are retrieved. Single lines from H, O I, Ca II, and Na I are also found. In the red extreme, in a region not strongly contaminated by telluric absorption bands, we also identify the Na I $\lambda\lambda 8183, 8195$ doublet, O I $\lambda 7774$ and $\lambda 8446$. Many lines, not marked in Fig. 13, can be attributed to a multitude of transitions from Ti II, as suggested also by Pastorello et al. (2019b).

5. Discussion and conclusion

AT 2025abao is the most recent example of a LRN in M 31, and the fourth in the last 40 years in this galaxy, with an observed LRN events rate of ≈ 0.1 yr $^{-1}$. All of them have peak absolute magnitudes in the range -8.5 to -10 mag. Brighter objects would have been easily detected, while fainter ones could be lurking among the Novae population. For comparison, only one object (V838 Mon) was discovered with this luminosity range in a similar lapse of time in the MW. Based on the estimations of Kochanek et al. (2014), we calculate an event rate of just 0.04 yr $^{-1}$ within the same magnitude range (0.07 yr $^{-1}$ of events brighter than -8.5 mag minus 0.03 yr $^{-1}$ brighter than -10 mag). Therefore, it seems that this kind of transients is more than twice as common in the Andromeda Galaxy than in the MW. The stellar mass of M 31 has been estimated to be $1 - 1.5 \times 10^{11} M_\odot$ (Barmby et al. 2006; Tamm et al. 2012; Kafle et al. 2018), while the equivalent for the Milky Way is $5 - 6 \times 10^{10} M_\odot$ (Licquia & Newman 2015; Bland-Hawthorn & Gerhard 2016). Hence, the Andromeda Galaxy is ~ 2.3 times more massive in stellar content and likely in number of stars. If we scale up the Galactic LRN rate in the -8.5 to -10 mag range from Kochanek et al. (2014) by this ratio, we find a rate that is very similar to the ob-

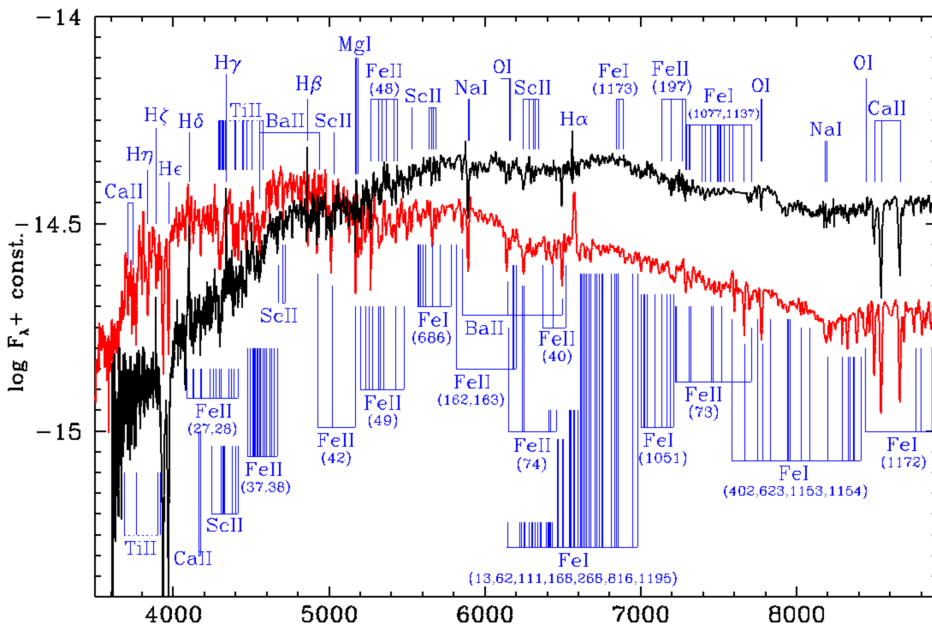


Fig. 13. Line identification on the mid-resolution spectrum of AT 2025abao taken with GTC+OSIRIS at +18.5 d (black), compared with a late time (+103 d) spectrum of LRN AT 2011kp (red line; from Pastorello et al. 2019b). Transitions from multiplets of neutral and singly ionized metals are marked.

served one. The LRN population is dominated by faint events, with 86 % of them having M_V between -3 and -8.5 mag, while those in the -8.5 to -10 mag range make only 8%, and the more luminous than -10 mag just 6% (however, Karambelkar et al. 2023 predict an even lower rate for these brighter events). Therefore, while we expect more than one LRN per year in M 31 (0.5 yr^{-1} for $M_V > -3$ mag according to Kochanek et al. 2014, times 2.3 equals $\approx 1.15 \text{ yr}^{-1}$), the rate of $M_V > -10$ events should only be $\sim 0.07 \text{ yr}^{-1}$ (or less according to Karambelkar et al. 2023), making them particularly rare.

Usually, the progenitors of LRNe are found to be yellow stars, often supergiants in the cases of the most luminous events (Mauerhan et al. 2015; Blagorodnova et al. 2017; Pastorello et al. 2021c; Blagorodnova et al. 2021; Cai et al. 2022b). However, the association of AT 2025abao with WNTR23bzdiq, a slowly variable AGB star (K25), makes it an exception. K25 interpreted this object as a common-envelope event and predicted a merging event as the outcome. AGB stars are so inflated that the outer layers of the atmosphere can be considered like a hot vacuum. Therefore, the companion star - especially if the mass ratio is particularly large - could pass through it, remaining engulfed within the envelope and without significantly changing the global colour of the system, which would remain red, as observed by K25.

We constructed the pre-outburst SED of AT 2025abao at the time of the last local peak in the light curve (at -333 d), before the optically thick phase. We used only the *gri*-bands data from ZTF, and since there was no contemporary *i*-band imaging, we assumed a constant $r-i$ colour from the only pre-outburst *i*-band public observation by ZTF (at -411 d, $r-i = +0.62$ mag). Subsequently, we corrected the SED for the same Galactic extinction adopted by K25 and accounting for their dust parameters obtained with the radiative transfer code DUSTY (Ivezic & Elitzur 1997) for the quiescent progenitor (i.e. $\tau_V = 2.7$, $T_s = 3500 \text{ K}$, $T_d = 1450 \text{ K}$, $Y = 2$, $\rho \propto r^{-2}$, silicate composition). These parameters, according to our DUSTY simulation, result in an additional circumstellar extinction of $A_V = 1.025$ mag. We compared this corrected SED with the ATLAS9 stellar atmospheric mod-

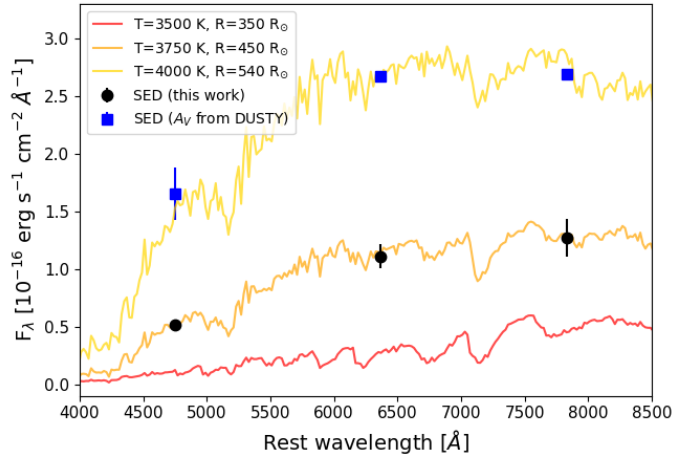


Fig. 14. Spectral energy distribution of the precursor of AT 2025abao, corrected for extinction in two different methods, compared to an ATLAS9 stellar atmospheric model. A good match is found with a model with $T_s = 4000 \text{ K}$ and $R_s = 540 R_\odot$. The model corresponding to the quiescent progenitor as determined by K25 is shown in red.

els by Castelli & Kurucz (2003)¹⁵. We adopted the models with $Z/Z_\odot = 1$ and $\log(g) = 0.0$. We find a good match with a model with a photospheric temperature of 4000 K , and a stellar radius of about $540 R_\odot$. The match of the ATLAS9 models to the precursor SED is shown in Fig. 14. These parameters are consistent with those of an orange supergiant, but also with an expanded AGB star, though hotter and more luminous ($\log(L_*/L_\odot) = 4.83$ vs. 4.20) than the progenitor parameters obtained by K25. If we instead adopt our distance and reddening estimates (Sect. 2), the corrected SED is fitted with a model having $T_s = 3750 \text{ K}$, a radius of $\sim 450 R_\odot$, and a corresponding $\log(L_*/L_\odot) = 4.57$, still hotter and more luminous than the quiescent progenitor.

We also used DUSTY to model the SED of the precursor of AT 2025abao observed by SPHEREx a few months before the outburst, at a phase close to the optical minimum. Since the

¹⁵ retrieved here: <https://archive.stsci.edu/hlsp/reference-atlases/cdbs/grid/ck04models/>

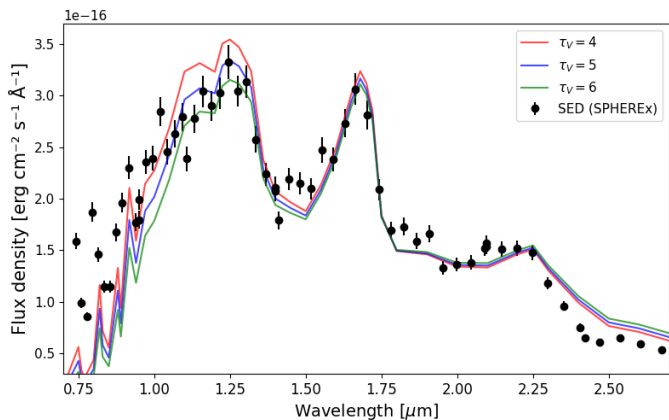


Fig. 15. Matches of the spectral energy distribution of the precursor of AT 2025abao observed by SPHEREx with three DUSTY models. They are constructed using a PHOENIX atmospheric model of $T_{\text{eff}} = 3100$ K extinguished by a dusty shell with silicate composition, $T_d = 1450$ K, and $\tau_V = 4, 5, 6$.

broad molecular absorptions at 1.4–1.5 and 1.8–2.2 μm are large deviations from a BB, we opted for an atmospheric model of a cool star as the radiation source. We adopted the PHOENIX models¹⁶ (Husser et al. 2013) with effective temperatures T_{eff} between 2500 and 3500 K, $[\text{Fe}/\text{H}] = 0.0$, and $\log(g) = 1.0$. Good matches are found for the model with $T_{\text{eff}} = 3100$ K and $\tau_V = 5 \pm 1$, which is higher than that found for the quiescent progenitor. The matches of the PHOENIX+DUSTY models to the SED from SPHEREx are shown in Fig. 15. The inner radius of the shell of dust is $\sim 1180 \pm 50 R_{\odot}$ (~ 5.5 AU), while the radius of the source is $350 R_{\odot}$, the same as the quiescent progenitor. However, the dust mass we obtain, following the procedures of Reguitti et al. (2026), is only $\approx 1.5 \times 10^{-8} M_{\odot}$, one order of magnitude lower than K25. This is due to the inner radius of the dust shell being much smaller.

K25 estimated a mass of the progenitor of $7 \pm 2 M_{\odot}$ based on evolutionary paths from MESA isochrones and stellar tracks. Using the empirical relation between absolute magnitude and the mass of the progenitor by Cai et al. (2022b) for an object with $M_V = -9.74 \pm 0.1$ mag during the plateau phase¹⁷, we obtain $7.5^{+6.1}_{-3.4} M_{\odot}$, in excellent agreement with their estimation. Based on the peak luminosity and similarities in the spectral evolution, we can also state that the progenitor mass of AT 2025abao must be similar to that of V838 Mon, which was $8 \pm 3 M_{\odot}$ (Pastorello et al. 2023; Tylynda 2005) and slightly more massive than that of AT 2019zhd ($6 M_{\odot}$ for Pastorello et al. 2019a; $3.4 M_{\odot}$ for Chen & Ivanova 2024).

AT 2025abao is a LRN exhibiting a plateau instead of a double-peaked light curve. Its progenitor has been established to be an early AGB (K25), hence an expanded star with an H-rich envelope. The photometric behaviour of AT 2025abao, similar to that of a Type IIP SN, can be explained with the recombination of a large quantity of H, previously ionized by the shocks following the merger of the two stars (MacLeod et al. 2017). Therefore, we propose that the observed dichotomy in LRNe – with some

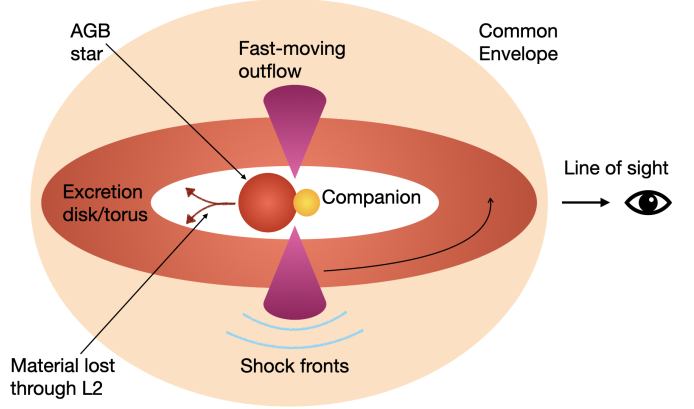


Fig. 16. Schematic sketch presenting the proposed scenario to explain the observed peculiar features in the $\text{H}\alpha$ line in the spectra at peak.

showing two clear light curve peaks (the first blue and the second red) and others with a plateau instead – is linked to the extent of the common envelope and the amount of H. Hence, systems having compact progenitors or with low H content would be responsible for double-peaked LRNe, whilst events with extended progenitors and massive outer H layers would produce LRNe with flat light curves (see also Howitt et al. 2020; Twum et al. 2026). The total mass of the system instead influences the luminosity of the event (as established by Kochanek et al. 2014; Blagorodnova et al. 2021; Cai et al. 2022b). Another possibility is that the plateau luminosity is maintained long by shocks produced by the collision of shells, together with the H-recombination (Matsumoto & Metzger 2022; Kirilov et al. 2025).

The narrow absorption visible on top of the $\text{H}\alpha$ profile in the spectra at maximum light (Fig. 10, right panel), with the red ‘horn’ fainter than the blue one, can be explained with a fast outflow far from being spherically symmetric (though it is still possible it could be axisymmetrical). We propose a scenario in which an excretion circumbinary disk (which may form if not all of the envelope is ejected; Ivanova et al. 2013b) or a torus-shaped structure surrounds the system. It would be observed at a nearly edge-on viewing angle, and would obscure the far receding side of the CSM, making the red-shifted portion of it more attenuated and thus fainter (see also Kirilov et al. 2025). We present a sketch of this scenario in Fig. 16.

In conclusion, it will be crucial to observe AT 2025abao years after the event with space telescopes, especially in the infrared domain (e.g. with JWST, as done by Karambelkar et al. 2025a, or with the forthcoming Roman, Akeson et al. 2019), to see what kind of outcome remains, and if the system returns to a state similar to the pre-LRN one, with an inflated red star. We note that a red (super)giant survivor was observed after the coalescence of a number of LRNe (Steinmetz et al. 2025; Reguitti et al. 2026). Future observations will also constrain the variability of the post-merger remnant, which may confirm whether the stellar components of the system had completely coalesced. In fact, very late-time observations of V838 Mon by Goranskij et al. (2020) revealed a slow brightening in the optical, which raises doubts if a complete merger really occurred in that system.

Data availability

The observed calibrated magnitudes are tabulated in the photometry tables, which are only available in electronic form at the CDS via anonymous ftp to cdsarc.u-strasbg.fr (130.79.128.5)

¹⁶ retrieved here: <https://pollux.oreme.org/explore/BT-Dusty/>

¹⁷ Obviously, AT 2025abao does not exhibit a genuine secondary red peak, but instead a long plateau. However, the relation of Cai et al. (2022b) can still be used, considering the V-band absolute magnitude at the end of the plateau. Consequently, in Appendix B, the Cai et al. (2022b) relation has been updated using also the AT 2025abao data.

or via <http://cdsweb.u-strasbg.fr/cgi-bin/qcat?J/A+A/>. All the spectra are released on the WISEREP interface (<https://www.wiserep.org/>).

Acknowledgements. AR acknowledges financial support from the GRAWITA Large Program Grant (PI D'Avanzo). AR, AP, GV, NER acknowledge financial support from the PRIN-INAF 2022 "Shedding light on the nature of gap transients: from the observations to the models". NER acknowledges support from the Spanish Ministerio de Ciencia e Innovación and the Agencia Estatal de Investigación 10.13039/501100011033 under the program Unidad de Excelencia María de Maeztu CEX2020-001058-M. TMR acknowledges support from the Research Council of Finland project 350458 and the Cosmic Dawn Center, which is funded by the Danish National Research Foundation under grant DNRF140. MDS is funded by the Independent Research Fund Denmark (grant nr. 10.46540/2032-00022B). YZC is supported by the National Natural Science Foundation of China (NSFC, Grant No. 12303054), the National Key Research and Development Program of China (Grant No. 2024YFA1611603), the Yunnan Fundamental Research Projects (Grant Nos. 202401AU070063, 202501AS070078), and the International Centre of Supernovae, Yunnan Key Laboratory (No. 202302AN360001). Based on observations collected at Copernico and Schmidt telescopes (Asiago Mount Ekar, Italy) of the INAF – Osservatorio Astronomico di Padova, and at the Galileo telescope of the Padova University (Asiago Mount Pennar, Italy). AR thanks Alessandro Fabris and Virginia Albanese for having participated to the observations with AFOSC. Support to ATLAS was provided by NASA grant NN12AR55G. Based on observations made with the NOT, owned and operated jointly by Aarhus University, the University of Turku, the University of Oslo, the University of Iceland and Stockholm University, under program 72-305 (PI Reguitti), and via the NUTS2 collaboration which is supported in part by the Instrument Centre for Danish Astrophysics, and the Finnish Centre for Astronomy with ESO via Academy of Finland grant nr. 306531. Based on observations made with the GTC. Based in part on observations made at the TNG, operated by INAF, under program A50TAC_41 (PI Valerini). All three telescopes are installed at the Spanish Observatorio del Roque de los Muchachos of the Instituto de Astrofísica de Canarias, on the island of La Palma. We acknowledge the use of data from the Swift data archive. FR is grateful to iTelescope.Net for providing observing time to use their remote telescopes and to the AAVSO who made it possible to use the AAVSOnet telescopes.

References

Addison, H., Blagorodnova, N., Groot, P. J., et al. 2022, MNRAS, 517, 1884

Ahumada, R., Allende Prieto, C., Almeida, A., et al. 2020, ApJS, 249, 3

Akeson, R., Armus, L., Bachelet, E., et al. 2019, arXiv e-prints, arXiv:1902.05569

Akeson, R., Dubois-Felsmann, G. P., Crill, B. P., et al. 2025, arXiv e-prints, arXiv:2511.15823, submitted to ApJS

Barmby, P., Ashby, M. L. N., Bianchi, L., et al. 2006, ApJ, 650, L45

Bellm, E. C., Kulkarni, S. R., Graham, M. J., et al. 2019, PASP, 131, 018002

Blagorodnova, N., Karambelkar, V., Adams, S. M., et al. 2020, MNRAS, 496, 5503

Blagorodnova, N., Klencki, J., Pejcha, O., et al. 2021, A&A, 653, A134

Blagorodnova, N., Kotak, R., Polshaw, J., et al. 2017, ApJ, 834, 107

Bland-Hawthorn, J. & Gerhard, O. 2016, ARA&A, 54, 529

Bock, J. J., Aboobaker, A. M., Adamo, J., et al. 2025, arXiv e-prints, arXiv:2511.02985, accepted by ApJ

Bond, H. E., Henden, A., Levay, Z. G., et al. 2003, Nature, 422, 405

Boschi, F. & Munari, U. 2004, A&A, 418, 869

Cai, Y., Reguitti, A., Valerini, G., & Wang, X. 2022a, Universe, 8, 493

Cai, Y. Z., Pastorello, A., Fraser, M., et al. 2019, A&A, 632, L6

Cai, Y. Z., Pastorello, A., Fraser, M., et al. 2022b, A&A, 667, A4

Castelli, F. & Kurucz, R. L. 2003, in IAU Symposium, Vol. 210, Modelling of Stellar Atmospheres, ed. N. Piskunov, W. W. Weiss, & D. F. Gray, A20

Chemin, L., Carignan, C., & Foster, T. 2009, ApJ, 705, 1395

Chen, Z. & Ivanova, N. 2024, ApJ, 963, L35

Fabregat, J., Peris, V., Lozano, A., & Comejero, J. 2025, ATel, 17527, 1

Falco, E. E., Kurtz, M. J., Geller, M. J., et al. 1999, PASP, 111, 438

Förster, F., Cabrera-Vives, G., Castillo-Navarrete, E., et al. 2021, AJ, 161, 242

Fraser, M. 2020, Royal Society Open Science, 7, 200467

Fraser, M., Kotak, R., Magill, L., Smartt, S. J., & Pastorello, A. 2011, ATel, 3574

Goranskij, V. P., Barsukova, E. A., Burenkov, A. N., et al. 2020, Astrophysical Bulletin, 75, 325

Goranskij, V. P., Barsukova, E. A., Spiridonova, O. I., et al. 2016, Astrophysical Bulletin, 71, 82

Graham, M. J., Kulkarni, S. R., Bellm, E. C., et al. 2019, PASP, 131, 78001

Guidolin, F., Pastorello, A., Stritzinger, M. D., et al. 2026, submitted to A&A

Henden, A. A. 2019, JAAVSO, 47, 130

Howitt, G., Stevenson, S., Vigna-Gómez, A., et al. 2020, MNRAS, 492, 3229

Hui, H., Bock, J. J., Condon, S., et al. 2026, arXiv e-prints, arXiv:2602.09139

Husser, T. O., Wende-von Berg, S., Dreizler, S., et al. 2013, A&A, 553, A6

Ivanova, N., Justham, S., Avendano Nandez, J. L., & Lombardi, J. C. 2013a, Science, 339, 433

Ivanova, N., Justham, S., Chen, X., et al. 2013b, A&A Rev., 21, 59

Ivezic, Z. & Elitzur, M. 1997, MNRAS, 287, 799

Kafle, P. R., Sharma, S., Lewis, G. F., Robotham, A. S. G., & Driver, S. P. 2018, MNRAS, 475, 4043

Kankare, E., Kotak, R., Pastorello, A., et al. 2015, A&A, 581, L4

Karambelkar, V., Kasliwal, M., Lau, R. M., et al. 2025a, arXiv e-prints, arXiv:2508.03932, submitted to ApJ

Karambelkar, V. R., Kasliwal, M. M., Blagorodnova, N., et al. 2023, ApJ, 948, 137

Karambelkar, V. R., Kasliwal, M. M., De, K., et al. 2025b, ApJ, 993, 109

Kechin, Y., Lipunov, V., Gorbovskoy, E., et al. 2025, Transient Name Server Discovery Report, 2025-4205, 1

Kirilov, A., Calderón, D., Pejcha, O., & Duffell, P. C. 2025, ApJ, 994, L41

Kochanek, C. S., Adams, S. M., & Belczynski, K. 2014, MNRAS, 443, 1319

Kulkarni, S. R., Ofek, E. O., Rau, A., et al. 2007, Nature, 447, 458

Kurtenkov, A. A., Peshev, P., Tomov, T., et al. 2015, A&A, 578, L10

Licquia, T. C. & Newman, J. A. 2015, ApJ, 806, 96

Lipunov, V. M., Blinnikov, S., Gorbovskoy, E., et al. 2017, MNRAS, 470, 2339

MacLeod, M., De, K., & Loeb, A. 2022, ApJ, 937, 96

MacLeod, M., Macias, P., Ramirez-Ruiz, E., et al. 2017, ApJ, 835, 282

Martini, P., Wagner, R. M., Tomaney, A., et al. 1999, AJ, 118, 1034

Mason, E., Diaz, M., Williams, R. E., Preston, G., & Bensby, T. 2010, A&A, 516, A108

Matsumoto, T. & Metzger, B. D. 2022, ApJ, 938, 5

Mauerhan, J. C., Van Dyk, S. D., Graham, M. L., et al. 2015, MNRAS, 447, 1922

Metzger, B. D. & Pejcha, O. 2017, MNRAS, 471, 3200

Mikolajczyk, P. J., Wyrykowska, L., Kotysz, K., et al. 2026, TNSAN, 21, 1

Mould, J., Cohen, J., Graham, J. R., et al. 1990, ApJ, 353, L35

Munari, U., Henden, A., Kiyota, S., et al. 2002, A&A, 389, L51

Pastorello, A. & Fraser, M. 2019, Nature Astronomy, 3, 676

Pastorello, A., Fraser, M., Valerini, G., et al. 2021a, A&A, 646, A119

Pastorello, A., Fraser, M., Valerini, G., et al. 2021b, A&A, 646, A119

Pastorello, A., Mason, E., Taubenberger, S., et al. 2019a, A&A, 630, A75

Pastorello, A., Mason, E., Taubenberger, S., et al. 2019b, A&A, 630, A75

Pastorello, A., Valerini, G., Fraser, M., et al. 2021c, A&A, 647, A93

Pastorello, A., Valerini, G., Fraser, M., et al. 2023, A&A, 671, A158

Pejcha, O. 2014, ApJ, 788, 22

Pejcha, O., Metzger, B. D., & Tomida, K. 2016a, MNRAS, 461, 2527

Pejcha, O., Metzger, B. D., & Tomida, K. 2016b, MNRAS, 455, 4351

Rayner, J. T., Cushing, M. C., & Vacca, W. D. 2009, ApJS, 185, 289

Reguitti, A., Pastorello, A., & Valerini, G. 2026, A&A, 706, A154

Schlafly, E. F. & Finkbeiner, D. P. 2011, ApJ, 737, 103

Shingles, L., Smith, K. W., Young, D. R., et al. 2021, TNSAN, 7, 1

Skopal, A., Shugarov, S., Tatarnikov, A. A., et al. 2025, ATel, 17476, 1

Smith, N., Andrews, J. E., Van Dyk, S. D., et al. 2016, MNRAS, 458, 950

Steinmetz, T., Kamiński, T., Melis, C., et al. 2025, A&A, 699, A316

Taguchi, K. & Maeda, K. 2025a, ATel, 17468, 1

Taguchi, K. & Maeda, K. 2025b, TNSCR, 2025-4414, 1

Tamm, A., Tempel, E., Tenjes, P., Tihhonova, O., & Tuvikene, T. 2012, A&A, 546, A4

Tonry, J. L., Denneau, L., Heinze, A. N., et al. 2018, PASP, 130, 064505

Tranin, H., Blagorodnova, N., Karambelkar, V., et al. 2025, A&A, 695, A226

Twum, A. A. G., Vigna-Gómez, A., MacLeod, M., et al. 2026, arXiv e-prints, arXiv:2602.10211

Tylenda, R. 2005, A&A, 436, 1009

Tylenda, R., Crause, L. A., Górný, S. K., & Schmidt, M. R. 2005, A&A, 439, 651

Tylenda, R., Hajduk, M., Kamiński, T., et al. 2011, A&A, 528, A114

Tylenda, R., Kamiński, T., Udalski, A., et al. 2013, A&A, 555, A16

Williams, S. C., Darnley, M. J., Bode, M. F., & Steele, I. A. 2015, ApJ, 805, L18

¹ INAF – Osservatorio Astronomico di Padova, Vicolo dell’Osservatorio 5, I-35122 Padova, Italy

² INAF – Osservatorio Astronomico di Brera, Via E. Bianchi 46, I-23807 Merate (LC), Italy

³ American Association of Variable Star Observers (AAVSO), 185 Alewife Brook Parkway, Suite 410 Cambridge, MA 02138 USA

⁴ Università degli Studi di Padova, Dipartimento di Fisica e Astronomia, Vicolo dell’Osservatorio 3, 35122 Padova, Italy

⁵ Yunnan Observatories, Chinese Academy of Sciences, Kunming 650216, P.R. China

⁶ International Centre of Supernovae, Yunnan Key Laboratory, Kunming 650216, P.R. China

⁷ Institute of Space Sciences (ICE, CSIC), Campus UAB, Carrer de Can Magrans s/n, 08193 Barcelona, Spain

⁸ Department of Physics and Astronomy, University of Turku, 20014 Turku, Finland

⁹ INAF – Osservatorio Astronomico di Trieste, Via G.B. Tiepolo 11, 34143 Trieste, Italy

¹⁰ Cosmic Dawn Center (DAWN), Niels Bohr Institute, University of Copenhagen, Jagtvej 128, 2200 København N, Denmark

¹¹ Department of Physics and Astronomy, Aarhus University, Ny Munkegade 120, DK-8000 Aarhus C, Denmark

Appendix A: Lines in the Na I D region in the Echelle spectra

In the first Echelle spectrum of AT 2025abao at -3.4 d (Figure A.1, top panel), a prominent absorption feature with a profile and intensity similar to the Na I D 2 line due to the transient is visible at 5890.9 Å (in the host galaxy rest frame). This has been tentatively identified in Figure A.1 (top panel) as the transition Na I D 2 from a third Na I doublet, redshifted by ~ 50 km s $^{-1}$ with respect to that of the LRN. However, the corresponding Na I D 1 transition, which would be located at 5896.9 Å, is not detected. Therefore, we believe that this feature is not an additional Na I D component, but most likely an absorption metal line. One possibility (though uncertain) is Fe II $\lambda 5891.48$ (multiplet 211), which is consistent with the detection of other Fe II lines in the spectrum. However, no other Fe II lines from the same ionization stage has been found.

In the second Echelle spectrum at $+33.6$ d (Figure A.1, bottom panel), the $\lambda 5890.9$ line is still present, but a new absorption is now visible at 5896.9 Å, which is fortuitously at the expected position of the Na I D 1 transition assuming that the doublet is redshifted by 50 km s $^{-1}$ with respect to the transient. However, accounting that more absorption lines of metals in neutral state have appeared in this phase, as the continuum temperature decreases, we tentatively identify this new line as Fe I $\lambda 5896.74$. Though an identification as V II $\lambda 5897.54$ is also possible, as absorption bands from the VO molecule are observed in the spectra at later phases.

Appendix B: Updated progenitor mass – luminosity relation

Considering the progenitor of AT 2025abao identified in archival images before the outburst, and its mass determined independently by K25, we can add it to the sample of objects used by Cai et al. (2022b) to derive the empirical relation between the progenitor mass and V -band absolute magnitude at the second peak (or during the plateau phase) for LRNe, with the goal of updated the with the robust data inferred for AT 2025abao. Adopting their estimate of $7 \pm 2 M_\odot$, and our value of $M_{V,plateau} \simeq -9.74 \pm 0.1$ mag, the updated Mass-Luminosity relation becomes:

$$\log(M/M_\odot) = (-0.172 \pm 0.017)M_V(\text{mag}) - (0.811 \pm 0.042). \quad (\text{B.1})$$

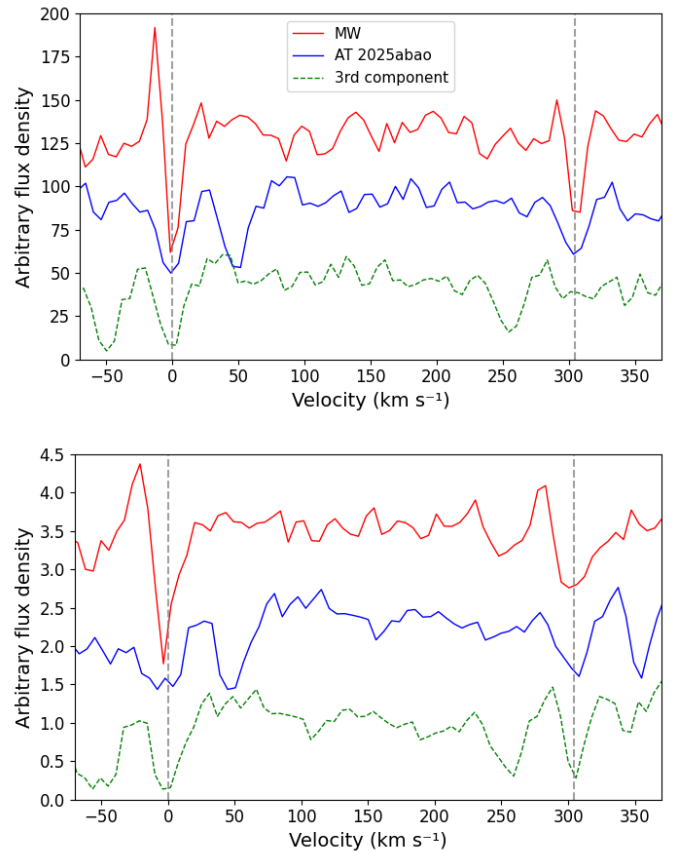


Fig. A.1. Zoom in on the Na I D spectral region in the Echelle spectra. The Na I D doublets of the Milky Way (red solid line) and that of the LRN (blue solid line) are plotted in the velocity space relative to the $\lambda 5890$ line (Na I D 2). Top: -3.4 d spectrum. The feature observed at $\lambda 5890.9$, indicated as 3rd component (green dashed line), is also shown at zero velocity. Adopting a tentative classification as an additional Na I D 2 component redshifted by ~ 50 km s $^{-1}$ (e.g., from a gas cloud along the line of sight), we note however that the corresponding Na I D 1 line is missing in this early spectrum. Bottom: $+33.6$ d spectrum. While the $\lambda 5890.9$ feature is still visible, a new line appears at $\lambda 5896.9$ at the expected wavelength of Na I D 1, that we preferentially identify as an Fe I or a V II transition (see text).

Appendix C: Complementary tables

Table C.1. Observational facilities and instrumentation used in our photometric follow-up of AT 2025abao.

Telescope	Location	Instrument	Filters
<i>Swift</i> (0.3m)	Space	UVOT	<i>UV</i> filters+ <i>UBV</i>
T21 (0.43m)	Utah	CCD	<i>BVR_CI_C</i>
ATLAS (0.50m)	Mauna Kea	ACAM1	<i>c, w, o</i>
T11 (0.51m)	Utah	CCD	<i>BVR_CI_C</i>
MPO61 (0.61m)	Texas	CCD, CMO	<i>BVgriz</i>
Schmidt (0.67m)	Asiago	Moravian	<i>uBVgri</i>
Oschin (1.20m)	Palomar	ZTF	<i>gr</i>
Copernico (1.82m)	Asiago	AFOSC	<i>uBVgriz</i>
NOT (2.56m)	La Palma	ALFOSC	<i>uBVgriz</i>
NOT (2.56m)	La Palma	NOTCam	<i>JHKs</i>

Table C.2. Log of the spectroscopic observations of AT 2025abao.

Date	MJD	Phase (d)	Spectral range (Å)	Resolution	Telescope + Instrument + Grism
2025-10-28	60976.90	-9.4	4100-8390	<i>R</i> ~ 200	BL41 0.2m + FOSC-E5535
2025-10-29	60977.61	-8.7	4050-8100	<i>R</i> ~ 500	Seimei 3.8m + KOOLS-IFU (★)
2025-10-31	60979.72	-6.6	4050-8100	<i>R</i> ~ 500	Seimei 3.8m + KOOLS-IFU (★)
2025-11-03	60982.86	-3.4	3660-7120	<i>R</i> ~ 20,000	Copernico 1.82m + Echelle
2025-11-03	60982.89	-3.4	3500-7580	<i>R</i> ~ 400	Galileo 1.22m + B&C + 300tr
2025-11-04	60983.75	-2.5	3400-7880	<i>R</i> ~ 400	Galileo 1.22m + B&C + 300tr
2025-11-05	60984.89	-1.4	3430-7880	<i>R</i> ~ 400	Galileo 1.22m + B&C + 300tr
2025-11-06	60985.79	-0.5	3500-8040	<i>R</i> ~ 450	Galileo 1.22m + B&C + 300tr
2025-11-07	60986.01	-0.3	3700-7130	<i>R</i> ~ 900	NOT 2.56m + ALFOSC + gr7
2025-11-07	60986.03	-0.3	5680-8590	<i>R</i> ~ 1,300	NOT 2.56m + ALFOSC + gr8
2025-11-10	60989.01	+2.7	3700-7130	<i>R</i> ~ 900	NOT 2.56m + ALFOSC + gr7
2025-11-10	60989.02	+2.7	5680-8590	<i>R</i> ~ 1,100	NOT 2.56m + ALFOSC + gr8
2025-11-16	60996.04	+9.7	3400-9720	<i>R</i> ~ 400	NOT 2.56m + ALFOSC + gr4
2025-11-23	61002.98	+16.7	6190-7840	<i>R</i> ~ 1,100	TNG 3.58m + DOLORES + VHRR
2025-11-24	61003.01	+16.7	3430-8120	<i>R</i> ~ 350	TNG 3.58m + DOLORES + LRB
2025-11-25	61004.82	+18.5	3600-10100	<i>R</i> ~ 2,100	GTC 10.4m + OSIRIS + R2500U/V/R/I
2025-12-02	61011.05	+24.7	3700-9200	<i>R</i> ~ 300	NOT 2.56m + ALFOSC + gr4
2025-12-10	61019.89	+33.6	3660-7110	<i>R</i> ~ 20,000	Copernico 1.82m + Echelle
2025-12-11	61020.98	+34.7	4870-9800	<i>R</i> ~ 370	Copernico 1.82m + AFOSC + VPH6
2025-12-22	61031.02	+44.7	3750-9200	<i>R</i> ~ 400	NOT 2.56m + ALFOSC + gr4
2025-12-31	61040.93	+54.6	3750-8900	<i>R</i> ~ 300	NOT 2.56m + ALFOSC + gr4
2026-01-12	61052.74	+66.4	4870-8950	<i>R</i> ~ 250	Copernico 1.82m + AFOSC + VPH6
2026-01-23	61063.90	+77.6	3850-9000	<i>R</i> ~ 300	NOT 2.56m + ALFOSC + gr4

Notes. The phases reported are relative to the *g*-band first maximum (MJD 60986.3). (★) Spectra presented by [Taguchi & Maeda \(2025a\)](#).